International Journal of Non-Linear Mechanics ∎ (∎∎∎∎) ∎∎∎–∎∎∎

Contents lists available at ScienceDirect

International Journal of Non-Linear Mechanics

journal homepage: www.elsevier.com/locate/nlm

Hyperelastic modeling of location-dependent human distal femoral cartilage mechanics

Jessica M. Deneweth [a,*], Ellen M. Arruda [b,c,d], Scott G. McLean [a]

[a] School of Kinesiology, University of Michigan, 401 Washtenaw Avenue, Ann Arbor, MI 48109, USA
[b] Department of Mechanical Engineering, University of Michigan, 2350 Hayward Ave., Ann Arbor, MI 48109, USA
[c] Department of Biomedical Engineering, University of Michigan, 2200 Bonisteel Blvd., Ann Arbor, MI 48109, USA
[d] Program in Macromolecular Science & Engineering, University of Michigan, 2300 Hayward Ave., Ann Arbor, MI 48109, USA

ARTICLE INFO

Article history:
Received 27 January 2014
Received in revised form
24 June 2014
Accepted 29 June 2014

Keywords:
Eight-chain network
Hyperelastic
Modeling
Cartilage mechanics
Knee
Osteoarthritis

ABSTRACT

Knee articular cartilage exhibits complex mechanical behavior, even under high strain rates, which poses a challenge to developing accurate and efficient cartilage models. In particular, the tissue's stress–strain response is non-linear and the stiffness of the response is location-dependent. Hyperelastic models such as those of Alan Gent and others have increasingly found use in soft tissue biomechanics. Recently, a hyperelastic statistical chain network model representing the transverse isotropy of the collagen matrix in the superficial tangential zone has been developed. The model successfully simulated the 100% strain/s unconfined compression response of human proximal tibial cartilage. Moreover, spatial variations in the tangent modulus to the nominal stress–strain curve taken at 10% strain were reflected in the variability of a single parameter of the model. Given the success of the model, we desired to determine whether these outcomes are equally applicable to healthy human distal femoral cartilage so that a complete model of tibiofemoral joint cartilage can be developed. The transversely isotropic model was employed along with two other hyperelastic chain network models to determine which model best simulated unconfined compression data for healthy distal femoral cartilage. The transversely isotropic model fit the data excellently ($R^2=0.999$). The model was subsequently simplified to depend on a single parameter and reapplied to the dataset. The modified model maintained an excellent fit to the data ($R^2=0.999$), and its single parameter varied in a statistically similar regional pattern ($p<0.05$) to the experimentally-obtained elastic modulus of the tissue. Outcomes suggest that this model is suitable for modeling the spatially-varying, non-linear mechanics of healthy human distal femoral cartilage. Implementation of this constitutive relation within computational models of the knee will provide novel insight into the relationship between joint mechanics, cartilage loading, and knee osteoarthritis development.

1. Introduction

Knee osteoarthritis (OA)[1] afflicts 14% of the US population over the age of 26 and 37% of the population over age 60, yet it remains a poorly understood disease [1]. Computational knee models afford a powerful research tool for investigating how the disease initiates and progresses [2–4]. Computational studies in which joint kinematics and kinetics are systematically varied and the effect on cartilage stress is determined can indicate which loading patterns are most likely to initiate and/or promote OA. However, the effectiveness of these models depends on the accuracy of the constitutive relations describing the many structures making up the knee. In the case of OA, in which the articular cartilage (AC)[2] is heavily affected, the AC material model is particularly important [5].

Selection of a material model requires balancing multiple criteria, such as correct mechanical response for loading conditions of interest, use of parameters with physical meaning that reveal insights into underlying mechanisms, and computational efficiency, e.g, short running time and minimal number of

* Corresponding author. Tel.: +1 248 568 6369; fax: +1 734 764 5237.
E-mail address: jmden@umich.edu (J.M. Deneweth).

[1] OA: osteoarthritis.

[2] AC: articular cartilage.

http://dx.doi.org/10.1016/j.ijnonlinmec.2014.06.013
0020-7462/

parameters [6,7]. For the study of OA, appropriate loading conditions are those associated with walking and other activities of daily living [8,9]. During level-ground walking knee cartilage undergoes compressive strains at a relatively high strain rate of 1 strain/s and peak strains near 20% [10,11], which can be challenging deformation parameters for popular AC models, e.g., the linear biphasic model and its derivatives [6,12,13].

The interaction of the three primary constituents of AC—collagen fibrils, large proteoglycan aggregates, and water containing mobile ions—gives rise to the tissue's mechanical response [14,15]. At equilibrium, the negatively-charged proteoglycans create a swelling pressure in the tissue, which is counteracted by tensile forces in the collagen network [16,17]. When compressed, fluid stress rises causing fluid to flow out of the tissue until equilibrium is re-established [18,19]. Fluid flow is resisted by electrostatic interactions with the proteoglycans and the physical impediments of the collagen matrix, producing a complex viscous response [18,20]. However, for the very short loading times that characterize typical human activity negligible fluid flow occurs. In this case, the tissue deforms nearly isochorically, with the amount of deformation governed by the mechanics of the collagen matrix [13,21–23]. Thus, the high strain-rate loading response of healthy AC may be successfully modeled by focusing on the short-term elasticity of the collagen network, without incorporating viscous effects or the contribution of proteoglycans.

The collagen network is characterized by non-linear elasticity [24], suggesting that a non-linear elastic model, such as a hyperelastic statistical chain network model, could be used to model the high strain-rate loading response of AC. Current linear elastic model are limited in their ability to fully represent the collagen network [19,25]. In contrast, hyperelastic statistical chain network models have successfully modeled high strain-rate, finite deformations of biological tissues containing collagen, such as aortic valve, skin, myocardium, tendon, and ligament [26–29]. The physical structure of these models is analogous to the collagen network that forms the backbone of the cartilage matrix [30,31]. These models require a small number of physically-meaningful parameters, enabling them to be executed in short computational times [26,32–34]. Taken together, these findings indicate that a statistical chain network model would be a viable model for high-strain rate loading of human knee cartilage. Other similar approaches to non-linear elasticity requiring a limited number of parameters to capture the full three-dimensional response of soft tissues are also becoming increasingly popular in soft tissue biomechanics. Although there are several notable models in this group, it behooves us to mention Alan Gent's elegant 1996 model [35].

Recently, it was determined that a transversely isotropic eight-chain network with freely jointed chains could simulate the 1 strain/s uniaxial compression response of healthy human tibial plateau cartilage with high accuracy ($R^2=0.999$) [32]. The transverse isotropy of the model reflects the anisotropy of the superficial tangential zone (STZ)[3] of cartilage [31,36], which is the zone that most influences the mechanical response of the AC matrix [21]. High accuracy was maintained when the model was reduced to dependence on a single parameter that related to the volume density of the solid collagen matrix. Furthermore, experimentally-determined regional variations in the tissue's linear elastic modulus at 10% strain were captured by this single parameter. Consequently this material model would be highly useful for evaluating the role of regional loading patterns on the development of OA [9,37,38]. It is plausible that a similar model would be equally effective at modeling the femoral cartilage of the knee.

With the above facts in mind, we currently aimed to evaluate three statistical chain-network models, including the transversely isotropic eight-chain network of freely-jointed chains, against healthy human distal femoral cartilage. The goal was to provide a complete material model for healthy human tibiofemoral joint cartilage that can be readily implemented into whole-knee computational modeling schemes. The first aim of the study was to determine which of three statistical chain network models could successfully model the uniaxial compression response of distal femoral AC. We hypothesized that the transversely-isotropic eight-chain network model, which was successful in representing regional tibial cartilage behaviors, would be the most successful of the three models. The second aim was to determine whether the model that best fit the data could represent the regional mechanical properties of the femoral AC via a single parameter. We hypothesized that variations in C_R, the parameter that reflects the chain density of the material, would match documented regional variations in the elastic tangent modulus at 10% nominal strain of the AC.

2. Methods

2.1. Material models

Three material models were evaluated for this study: the eight-chain isotropic network with freely-jointed chains (FJC)[4] [39], the eight-chain isotropic network with MacKintosh chains (MAC)[5] [33,40], and the eight-chain transversely isotropic network with freely-jointed chains (TI)[6] [32]. Each model can be described by (1) the constitutive relation used to model a single chain molecule, i.e., a single collagen fibril, and (2) the manner in which the chains are assembled together to the material network, i.e., the cartilage solid matrix. The following sections briefly describe two chain models (the freely-jointed chain and the MacKintosh chain), two network models (the eight-chain isotropic network and the eight-chain transversely isotropic network), how they were combined into the three chain-network models (FJC, MAC, TI) of interest, and how those models were implemented for the case of uniaxial compression.

2.1.1. Mechanical response of single collagen fibril

The freely-jointed chain [41] and the MacKintosh chain [40] represent two common chain models. These chains are suitable for the large, non-linear deformations that typically occur in biological tissues. The chains are considered entropy springs: each chain seeks the conformation that results in maximal entropy. Elongating the chain decreases its entropy and increases its strain energy. The freely-jointed chain can be modeled as N rigid links of length l (Fig. 1a). One end of the chain is fixed at the origin and the other end occupies a volume dv at a location $\boldsymbol{r}$ with probability $p(\boldsymbol{r})$:

$$\ln\ p(\boldsymbol{r}) = p_0 - N\left(\frac{r}{Nl}\beta_r + \ln\frac{\beta_r}{\sinh\ \beta_r}\right) \tag{1}$$

where p_0 is a constant, $r=|\boldsymbol{r}|$, $\beta_r=\mathscr{L}^{-1}(r/Nl)$, and $\mathscr{L}(x)=\coth x-1/x$ is the Langevin function. The inverse Langevin is commonly computed from the Padé approximation [42]:

$$\mathscr{L}^{-1}(x) = x\frac{(3-x^2)}{(1-x^2)} + O(x^6) \tag{2}$$

[3] STZ: superficial tangential zone.

[4] FJC: isotropic eight-chain network with freely-jointed chains.

[5] MAC: isotropic eight-chain network with MacKintosh chains.

[6] TI: transversely-isotropic eight-chain network with freely-jointed chains.

Please cite this article as: J.M. Deneweth, et al., Hyperelastic modeling of location-dependent human distal femoral cartilage mechanics, International Journal of Non-Linear Mechanics (2014), http://dx.doi.org/10.1016/j.ijnonlinmec.2014.06.013

Elongating the freely-jointed chain to vector length r requires a tensile force, f_{chain} [39]:

$$f_{chain} = \frac{k\Theta}{l}\beta_r \tag{3}$$

where the Padé approximation has been used to simplify the inverse Langevin, k is Boltzmann's constant, 1.38065×10^{-23} J K^{-1}, and Θ is the absolute temperature. Please refer to Arruda [39] for a complete derivation. In the freely-jointed chain the position of one link relative to the previous link is uncorrelated, i.e., all link angles have equal probability. Consequently the chain is highly flexible and its resting end-to-end length r_0 is much less than its contour length $L=Nl$ (Fig. 1a). The chain force remains low for small strains and then rapidly increases as the strain approaches the locking stretch, $\sqrt{N}$.

The MacKintosh model, in contrast, enforces a smooth, continuous curvature to the chain (Fig. 1b). Therefore, the chain is semiflexible and its initial length, r_0, is on the same order of magnitude as its maximum length, L. To enforce the curvature constraint, the model incorporates an additional parameter to those of the freely-jointed chain, the persistence length (l_P), which controls the chain's bending rigidity. As l_P increases, the molecule becomes less flexible and r_0 approaches L. The average length of the MacKintosh chain under no applied tension, $r_{f=0}$, can be related to L and l_P via [33]:

$$r_{f=0} = L\left(1 - \frac{L}{6l_P}\right) \tag{4}$$

Extending the chain to vector length r requires a tensile force, f_{chain}:

$$f_{chain} = \frac{k\Theta}{l_p}\left(\frac{1}{4(1-(r/L))^2}\right)\left(\frac{(L/l_p)-6(1-(r/L))}{(L/l_p)-2(1-(r/L))}\right) \tag{5}$$

where all constants are as defined previously. For a complete derivation, please refer to Palmer [33].

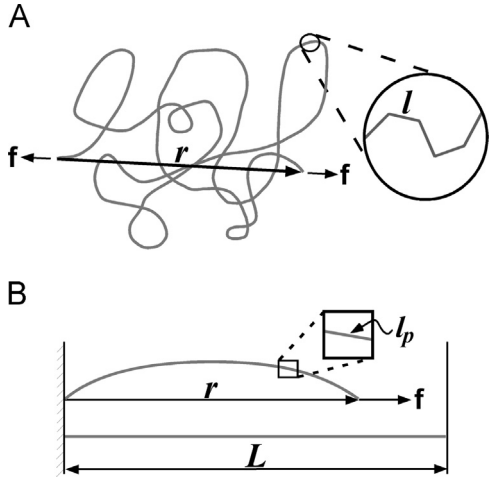

Fig. 1. Schematics of the (a) freely-jointed chain and (b) MacKintosh chain. The highly-flexible freely-jointed chain is composed of N rigid segments of length l. In contrast, the MacKintosh chain is constrained to have a smooth curvature as determined by the persistence length, l_p, and is less flexible than the freely-jointed chain. Both chains have a contour length, L. Adapted from Deneweth [32].

2.1.2. Mechanical response of the network

The eight-chain network [39] has been previously implemented with freely-jointed chains and with MacKintosh chains to model various biological materials, including skin, cardiac wall, breast, actin filament network, ligament, and cartilage [27,29,33,43–45]. In its isotropic form, the model can be visualized as a unit cube with eight chains emanating from the center of the cube and extending to each corner (Fig. 2). The chains stretch and rotate as the cube is deformed. If the principal directions of deformation remain constant throughout the deformation, the sides of the cube will maintain alignment with the principal stretch directions.

For the case of freely-jointed chains, Eq. (3) is incorporated into the isotropic eight-chain network to obtain the strain energy, U_{FJC}, for the FJC model:

$$U_{FJC} = nk\Theta N\left\{\frac{\lambda_{chain}}{\sqrt{N}}\beta_{chain} + \ln\frac{\beta_{chain}}{\sinh\ \beta_{chain}}\right\} \tag{6}$$

where n is the chain density, $\lambda_{chain} = (\lambda_1^2+\lambda_2^2+\lambda_3^2)^{1/2}/\sqrt{3}$, λ_i is the principal stretch in the ith direction ($i=1$, 2, 3), and $\beta_{chain} = \mathscr{L}^{-1}(\lambda_{chain}/\sqrt{N})$ [39].

For uniaxial compression, the nominal stress in the axial direction becomes [39]

$$T_{o1FJC} = \frac{nk\theta}{3}\frac{\sqrt{N}}{\lambda_{chain}}\mathscr{L}^{-1}\left(\frac{\lambda_{chain}}{\sqrt{N}}\right)(\lambda-(1/\lambda^2)) \tag{7}$$

where λ is the applied axial stretch and $\lambda_{chain}=[(\lambda^2+2/\lambda)/3]^{1/2}$. The model assumes incompressibility of the material, which is acceptable for healthy AC subjected to high strain rates because relative motion of the fluid with respect to the solid and fluid exudation are negligible [45–48]. Two material constants dictate the stress response: $C_R=nk\theta$, which reflects the chain density of the material and influences the initial modulus of linear elasticity

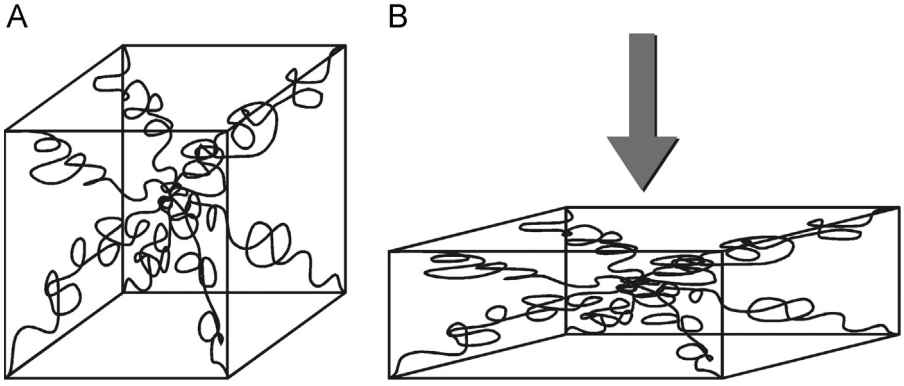

Fig. 2. The isotropic eight-chain network in its reference configuration (left) and deformed in uniaxial compression (right). The statistical chains rotate and stretch with applied deformations.

(i.e., the slope of the stress–strain curve as the strain approaches zero), and N, which dictates the locking stretch of the network.

Likewise, implementation of MacKintosh chains into the isotropic eight-chain network yields the strain energy for the MAC model [33]:

$$U_{Mac} = nk\Theta\left\{\frac{L}{4l_p y} + \ln(y) - \ln(L-2l_p y)\right\} \tag{8}$$

$$y = 1 - \frac{r}{L} = 1 - \frac{r_0\lambda_{chain}}{L} \tag{9}$$

where n, k, Θ, and λ_{chain} are defined identically to the FJC model. Assuming $r_0 = r_{f=0}$, the axial nominal stress is

$$T_{o_1 MAC} = \frac{nk\Theta}{3l_p}\frac{r_{f=0}}{\lambda_{chain}}\left[\frac{1}{4(1-(r_{f=0}\lambda_{chain}/L))^2}\right] \times\left[\frac{(L/l_p)-6(1-(r_{f=0}\lambda_{chain}/L))}{(L/l_p)-2(1-(r_{f=0}\lambda_{chain}/L))}\right](\lambda - 1/\lambda^2) \tag{10}$$

Since $r_{f=0}$ is a function of l_p and L (Eq. (2)), the response depends on only three material constants: $C_R = nk\theta$, l_p, and L.

Transversely isotropic [28,32] and orthotropic [26,49] eight-chain networks have recently been introduced. A transversely isotropic eight-chain network with freely-jointed chains has been shown to better simulate the uniaxial compression response in human tibial plateau cartilage than isotropic eight-chain network models [32]. This transversely isotropic model was a modification of the orthotropic eight-chain model of Bischoff [26] and will be used in the current study. The transversely isotropic case is derived by modifying the structure of the isotropic eight-chain model from a cube to a rectangular prism (Fig. 3). The side aligned with the principal compression axis has dimension a, which has been normalized by dividing by l. The remaining two sides, which lie in the plane perpendicular to the compression axis, have normalized dimension b. The ratio b:a indicates the degree of anisotropy of the tissue, with b:a=1 occuring for the isotropic case. The direction corresponding to the largest dimension will also exhibit the highest tensile modulus [26,49]. Additionally, incompressibility is not assumed but a bulk compressibility term is included to maintain near-incompressibility. The total strain energy of the transversely isotropic eight-chain configuration of freely jointed chains (TI) is given as [26,32]

$$U_{TI} = U_0 + \frac{nk\Theta}{4}\left(N\sum_{i=1}^{4}\left[\frac{\rho^{(i)}}{N}\beta_\rho^{(i)} + \ln\frac{\beta_\rho^{(i)}}{\sinh\beta_\rho^{(i)}}\right] - \frac{\beta_P}{\sqrt{N}}\ln[\lambda_{\mathbf{a}}^{a^2}\lambda_{\mathbf{b}}^{2b^2}]\right) + \frac{B}{\alpha^2}\{\cosh[\alpha(J-1)]-1\} \tag{11}$$

where U_0 is a constant; $\beta_\rho^{(i)} = \mathscr{L}^{-1}(\rho^{(i)}/N)$; $\beta_P = \mathscr{L}^{-1}(P/N)$; $P = \frac{1}{2}\sqrt{a^2+2b^2} = \sqrt{N}$ is the undeformed chain length; $\rho^{(i)}$ is the deformed length of the ith chain; $\lambda_{\mathbf{a}}$ and $\lambda_{\mathbf{b}}$ are the stretches along the axis of compression and the two axes perpendicular to the axis of compression, respectively; $J = \lambda_1\lambda_2\lambda_3$ is the ratio of the deformed volume to the original volume; B controls the bulk compressibility near J=1; and α is a constant that governs the curvature of the hydrostatic pressure versus volume curve for large volume changes.

The nominal axial stress for uniaxial deformation of the nearly incompressible transversely isotropic freely jointed eight-chain (TI) model is

$$T_{0_1 TI} = \frac{nk\theta}{4\lambda_1}\left(a^2\left[\frac{\lambda_1^2\beta_\rho}{\rho} - \frac{\beta_P}{\sqrt{N}}\right] - b^2\left[\frac{\lambda_2^2\beta_\rho}{\rho} - \frac{\beta_P}{\sqrt{N}}\right]\right) \tag{12}$$

where $\rho = \frac{1}{2}\sqrt{a^2\lambda_1^2 + 2b^2\lambda_2^2}$, $P = \sqrt{N} = \frac{1}{2}\sqrt{a^2+2b^2}$, and $\lambda_2 = \sqrt{J/\lambda_1}$. Small volume changes were assumed to agree with the near incompressibility of the tissue so α was set equal to unity [48]. The TI model requires three independent parameters in addition to $C_R = nk\theta$: a, b, and J.

2.2. Experimental data

Each model was simulated against uniaxial compression data using a method described previously [37]. Cylindrical, full-thickness explants of healthy AC were procured from 29 standardized tests sites of seven human femurs. Femurs were obtained from cadaveric Caucasian female donors whose cause of death was unlikely to compromise the knee joint (mean ± standard deviation age: 50 ± 3 years). Knees were stored at −20 °C until samples were procured. The femoral AC surface was isolated by thawing the knee overnight to room temperature, removing all soft tissue to expose the tibiofemoral and patellofemoral joints, and disarticulating the femur from the tibia and patella. Standardized grid patterns were fitted onto the trochlear (3 cells mediolateral × 3 cells proximodistal, typical cell size: 10 mm × 13 mm) and condylar (2 cells mediolateral × 5 cells proximodistal, typical cell size: 12 mm × 15 mm) surfaces such that a maximum AC surface area fell under the grid (Fig. 4) [32,50]. Cartilage samples were obtained from the center of each grid cell, which resulted in 9 trochlear samples and 20 condylar samples per knee. A 4-mm diameter round-hole hand punch was used to isolate the sample, and a surgical scalpel was employed to carefully separate the AC from the subchondral bone [51]. Each sample was stored in phosphate buffered saline solution at −20 °C until mechanical testing was performed. Freezing and thawing AC at this temperature has been found to preserve the samples' mechanical properties [52,53]. An India ink test was conducted prior to extraction to identify surface fibrillation [54]. Samples with surface damage were excluded from testing.

Explants were subjected to three trials of unconfined compression from 0% to 20% peak nominal strain at 1 strain/s, which

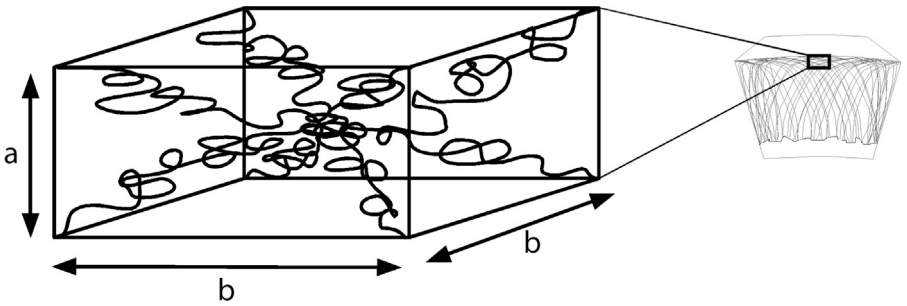

Fig. 3. The transversely isotropic model replicates the architecture of the collagen matrix in the STZ. The dimension a is aligned perpendicular to the cartilage surface, while the remaining two sides, each with dimension b, are parallel to the cartilage surface. As b increases relative to a, the orientation of the chains rotate to become more parallel to the cartilage surface. Correspondingly the tensile modulus in plane defined by the b dimensions increases while the tensile modulus along the a dimension decreases.

Please cite this article as: J.M. Deneweth, et al., Hyperelastic modeling of location-dependent human distal femoral cartilage mechanics, International Journal of Non-Linear Mechanics (2014), http://dx.doi.org/10.1016/j.ijnonlinmec.2014.06.013

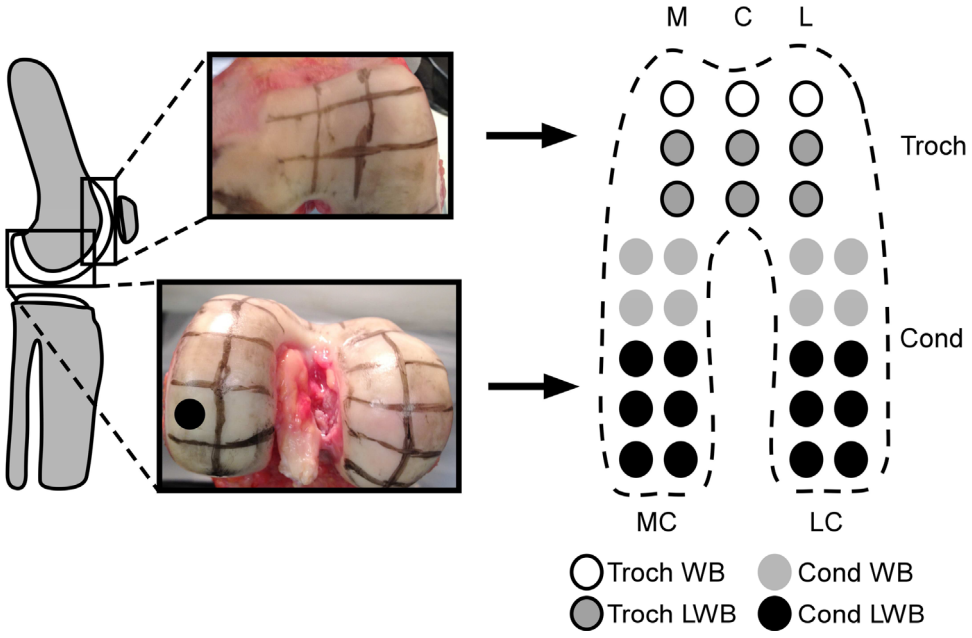

Fig. 4. (Left) Cartilage samples were extracted from the trochlea and condyles of each femur. A grid pattern was drawn onto each surface, and a sample was taken from the center of each grid cell (black circle). (Right) For statistical analysis, the 29 test sites (circles) were grouped by region (trochlea, Troch, $n=9$; condyles, Cond, $n=20$). Samples were grouped within region by mediolateral position and weightbearing frequency (WB/LWB). C: central trochlea, L: lateral trochlea, LC: lateral condyle, LWB: less-frequently loaded, M: medial trochlea, MC: medial condyle, WB: frequently loaded.

replicates the AC strain and strain rate associated with level-ground gait [10,11]. Testing was conducted with a custom high-rate uniaxial tester [37]. It contained a fixed dynamic load cell (Dytran Instruments, Chatsworth, CA; sensitivity: 120 mV/N) and a horizontal high-speed electric linear actuator (SMAC, Carlsbad, CA; positional accuracy: ± 0.001 mm) fixed at opposite ends of a PBS solution bath. Compression plates were mounted on the load cell and actuator (Dytran Instruments, Chatsworth, CA; diameter: 15.78 mm). A high-speed video camera (Photron USA, San Diego, CA; maximum frame rate: 5400 frames/s) was mounted above the testing apparatus to record deformation of the sample during each test.

Cartilage explants were thawed at room temperature, placed under a minimal tare load (0.2 N), and allowed to equilibrate for 10 min in the phosphate buffered saline bath prior to testing. A random speckle pattern was applied to the exposed explant surface with black India ink [37,55]. The sample underwent ten pre-conditioning cycles at the prescribed strain and strain rate. Subsequently three experimental trials of compression (compressed from 0% to 20% peak strain followed by immediate return to 0% strain) were conducted while synchronous force and video were recorded at 125 Hz. Several minutes were allowed between trials for the specimen to re-equilibrate.

Digital image correlation software was used to calculate average nominal axial strain, i.e., $\lambda-1$, via the local deformation of the speckle pattern [37,56]. Average nominal stress was computed by dividing the current force by the undeformed cross-sectional area. Axial nominal stress–strain curves were constructed and used as input data for model simulations. Additionally, the tangent modulus to the nominal stress vs. nominal strain curve at 10% strain ($E_{10\%}$) was extracted and averaged across trials [37]. This strain level was selected because it is representative of physiological cartilage strain experienced during walking and running [10,11].

2.3. Model simulations

Model simulations were conducted in Matlab (Mathworks, Natick, MA) using the third experimental data trial from each AC specimen. Inputs were the experimental strain, experimental stress, and an initial guess at the unknown model parameters: C_R and N for FJC; C_R, l_P, and L for MAC; and C_R, a, b, and J for TI. Since all parameters represent lengths, moduli, or a volume ratio, non-negative parameter values were required. A built-in non-linear least-squares optimization routine determined the model parameters that minimized the squared error between the experimental stress and model-predicted stress. Based on our previous work [32], we additionally constrained $a=1$ so that variations in b alone dictated the anisotropy of the tissue, $b \geq 1$ since a and b were normalized to l, and $J \leq 1$ [57,58]. The goodness of fit of each model was determined from:

$$R^2 = 1 - \frac{\sum_i (\sigma_{exp_i} - \sigma_{pred_i})^2}{\sum_i (\sigma_{exp_i} - \overline{\sigma}_{pred_i})^2} \tag{13}$$

where σ_{exp_i} is the experimental stress corresponding to the ith strain data point, σ_{pred_i} is the ith predicted stress, and $\overline{\sigma}_{pred}$ is the mean predicted stress.

2.4. Analysis of regional dependence

The best-fitting model (highest R^2) was simplified so that only C_R was a free parameter and the remaining parameters were held constant [32]. The optimization scheme was repeated in Matlab for all experimental trials for each AC specimen. The goodness of fit was calculated for each simulation via Eq. (13). Simulations with excellent fit to the data, $R^2 \geq 0.97$, were used for regional analysis. This high cut-off was selected so that the effect of C_R could be clearly assessed. Mean C_R was computed for the trochlea as a whole, the condyles as a whole, six sub-regions on the trochlea [the medial, central, and lateral frequently loaded, i.e., "weight-bearing" (WB),[7] and the medial, central, and lateral less-frequently loaded, i.e., less weightbearing (LWB),[8] sub-regions], and four sub-regions on the condyles [medial and lateral WB and LWB] (Fig. 4).

[7] WB: frequently loaded ("weightbearing") articular cartilage.
[8] LWB: less-frequently loaded ("less weightbearing") articular cartilage.

Please cite this article as: J.M. Deneweth, et al., Hyperelastic modeling of location-dependent human distal femoral cartilage mechanics, International Journal of Non-Linear Mechanics (2014), http://dx.doi.org/10.1016/j.ijnonlinmec.2014.06.013

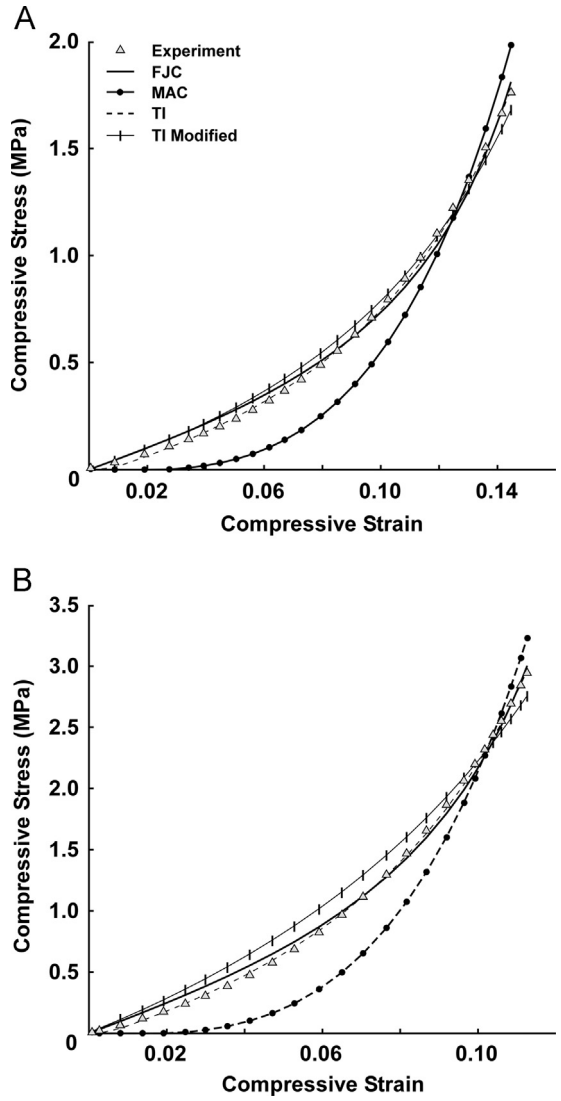

Fig. 5. Examples of unconfined compression data (triangles) with the simulated fit of each model. The TI Modified is the TI model with all parameters fixed except C_R. The TI model was most successful in fitting the experimental data.

Weightbearing and less weightbearing areas represented femoral cartilage contacting the opposing joint surface between 0° and 30° knee flexion and beyond 30° knee flexion, respectively [59–62].

Mean C_R of the trochlea and condyle primary regions were compared with repeated-measures analyses of variance (ANOVA). For the sub-regions, the main effect of side [medial, lateral, (central)] and contact frequency (WB, LWB) and the interaction of the two factors on C_R were evaluated with repeated-measures mixed model ANOVA. In the case of significant main effects or interactions ($p<0.05$), Bonferroni-adjusted pairwise comparisons were made. For comparison to experimental data, mean $E_{10\%}$ was calculated for each region of interest and submitted to the same statistical analysis. All statistical analyses were conducted with SAS 8.0 software (SAS Institute Inc., Cary, NC).

3. Results

3.1. Determination of best fitting model

The TI model consistently provided the best fit to the experimental data ($R^2=0.999$), followed by the FJC ($R^2=0.995$), and MAC models ($R^2=0.906$) (Fig. 5). The MAC model tended to underestimate the stress at low strain and overestimate it at high strain, whereas the FJC model slightly overestimated the stress at low strains but matched the stress at high strains. The mean and standard deviations for each model's parameters are presented in Table 1.

3.2. Analysis of regional dependence

3.2.1. Model

The TI model was used for the analysis of regional dependence as it had the highest R^2. The model was modified such that only C_R could vary by establishing the following parameter conditions: $a=1$ (from best-fit analysis), $b=1.348$ (mean for best-fit analysis), $J=1$ (incompressible). The goodness of fit remained high when the TI model was implemented with these modifications ($R^2=0.981$, Fig. 5).

Mean C_R is tabulated by knee and sub-region in Table 2. For regional analysis, 20.28% (100 out of 493 total) of simulations were excluded due to ($R^2<0.970$). C_R was significantly lower for the trochlea (0.533 ± 0.476 MPa) compared to the condyles (0.696 ± 0.517 MPa), $F(1,6)=10.42$, $p<0.05$. Within the trochlea, there was a significant effect of Side on C_R, $F(2,12)=10.79$, $p<0.01$ (Fig. 6). Pairwise comparisons determined no statistically significant difference between the medial and central one-thirds ($p=1.00$). However, the lateral one-third C_R was significantly larger than the medial and central thirds ($p<0.01$ for both cases). No statistically significant effect of Contact Frequency [$F(1,6)=0.74$, $p=0.422$] nor of the interaction of Side x Contact Frequency [$F(2,8)=0.98$, $p<0.418$] was found for the trochlea.

On the condyles, Side did not have a significant main effect of C_R although a trend of the lateral side being stiffer than the medial side was evident, $F(1,6)=4.07$, $p=0.090$. However, a significant main effect of Contact Frequency was determined, with WB sub-regions demonstrating significantly lower C_R than LWB regions, $F(1,6)=10.48$, $p<0.05$ (Fig. 7). No significant interaction of Side x Contact Frequency was determined. Fig. 8 depicts the regional variation of mean C_R across the femoral surface.

3.2.2. Experimental

Similar to the model result, $E_{10\%}$ was significantly lower for the trochlea relative to the condyles, $F(1,6)=30.54$, $p<0.05$. In the trochlea, there was a significant main effect of Side on $E_{10\%}$, $F(2,11)=9.79$, $p<0.01$, with $E_{10\%}$ of the lateral region significantly higher compared to the medial ($p<0.01$) and central ($p<0.05$) sub-regions. No significant difference was evident between the medial and central sub-regions ($p=0.466$). No statistically significant difference was present between WB and LWB sub-regions, $F(1,6)=0.02$, $p=0.886$, and there was no interaction of Side x Contact Frequency, $F(2,9)=1.61$, $p=0.253$. The condyles displayed a significant main effect of Contact Frequency on $E_{10\%}$, $F(1,6)=11.96$, $p<0.05$, with mean $E_{10\%}$ lower in WB compared to LWB. No significant main effect of Side, $F(1,6)=1.41$, $p=0.280$, or interaction of Side x Contact Frequency, $F(1,6)=0.52$, $p=0.499$, were detected. Fig. 8 shows the mean regional values for $E_{10\%}$ compared to C_R.

4. Discussion

In agreement with our first hypothesis, the TI model best modeled the AC nominal stress–strain response. The FJC model was slightly worse than the TI model but still a very good fit to the data. In contrast, the MAC model performed much worse than the other models in capturing the experimental results. In fact, the shape of the best-fit MAC curve was notably different from the TI and FJC curves, with lower stresses at low strains and higher

Please cite this article as: J.M. Deneweth, et al., Hyperelastic modeling of location-dependent human distal femoral cartilage mechanics, International Journal of Non-Linear Mechanics (2014), http://dx.doi.org/10.1016/j.ijnonlinmec.2014.06.013

Table 1
Mean and standard deviation of optimized parameters for the FJC, MAC, and TI models.

	FJC			MAC				TI			
	C_R (MPa)	N	R^2	C_R (MPa)	L	l_P	R^2	C_R (MPa)	b	J	R^2
Mean	0.053	1.143	0.995	5.045	4.207	5.792	0.906	0.370	1.348	0.994	0.999
SD	0.047	1.390	0.005	2.667	0.907	0.902	0.075	0.615	0.248	0.005	0.001

Table 2
Mean C_R (MPa) of modified TI model by knee and sub-region.

Knee	Trochlea						Condyles			
	M WB	C WB	L WB	M LWB	C LWB	L LWB	M WB	L WB	M LWB	L LWB
1	0.094	0.085	0.244	0.107	0.125	0.272	0.228	0.335	0.270	0.707
2	0.217	0.462	0.404	0.158	0.480	0.617	0.504	0.614	0.617	1.465
3		1.349	1.658	1.532	1.389	1.811	1.620	2.163	1.658	1.862
4	0.130	0.320		0.324	0.078	0.379	0.215	0.375	0.208	0.543
5	0.189		0.196	0.300	0.191	0.550	0.598	0.535	0.439	0.634
6	0.411	0.604	0.963	0.121	0.122	1.594	0.358	0.595	0.657	1.008
7	0.314	0.194	0.521	0.144	0.404	0.733	0.256	0.483	0.607	0.332

M – medial; C – central; L – lateral; WB – weightbearing; LWB – less weightbearing.
Blank cells indicate that no simulations with $R^2 > 0.970$ were conducted.

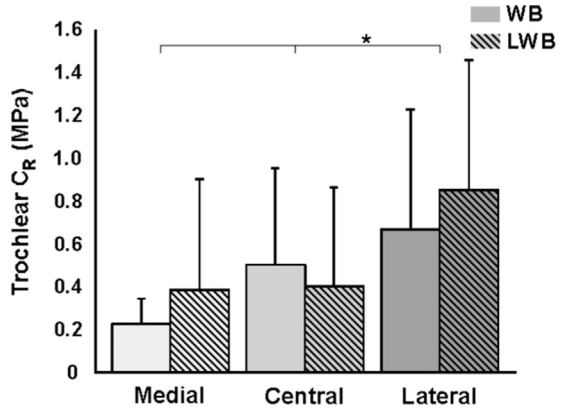

Fig. 6. Mean C_R across the six sub-regions of the trochlea. Bars indicate one standard deviation. Hatching indicates less weightbearing regions. The lateral weightbearing and less weightbearing sub-regions had significantly higher C_R compared to the medial and central sub-regions. No statistical differences were determined for weightbearing versus less weightbearing regions. These findings agree well with experimentally-determined cartilage moduli.

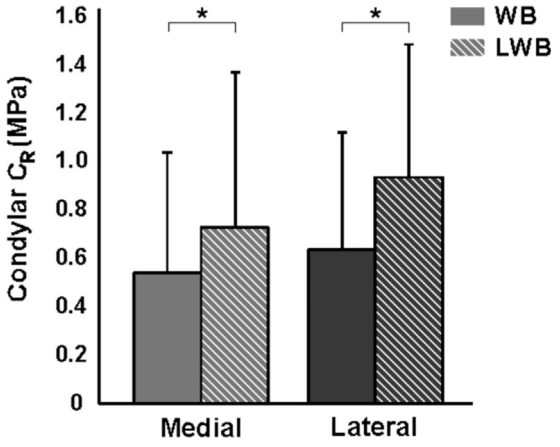

Fig. 7. Mean C_R across the four sub-regions of the condyles. Bars indicate one standard deviation. Hatching indicates less weightbearing regions. The weightbearing regions had significantly lower C_R compared to the less weightbearing regions. No statistical differences were determined between the medial and lateral regions. These findings agree well with the experimentally-determined cartilage moduli.

stresses at higher strains. The MacKintosh chains of the MAC model are quite different from the freely-jointed chains of the FJC and TI models, which likely accounts for the disparate model performances. The MAC model was developed for chains that are semi-flexible [33,40], whereas the FJC and TI assume flexible chains [26,39,41]. Additionally, the length of the undeformed configuration relative to its limiting extensibility differs among models. The undeformed configuration of the Mackintosh chain is near its limiting extensibility [40]. In contrast, the undeformed length of the freely-jointed chain is much less than its limiting extensibility [39,41]. Based on the results of the model simulations, it appears that type II collagen, which represents the most common collagen type found AC [63], is best represented by the freely-jointed chain utilized in the FJC and TI models.

Our second hypothesis was that the TI model could represent the regional mechanical properties of femoral AC via variations in C_R. The results of this study support this hypothesis. In the modified TI model $a=1$, $b=1.348$, $J=1$, and C_R was selected to optimize the simulated stress to the experimental stress. Model simulations against the entire experimental dataset produced values of C_R that varied regionally within each knee in a similar fashion to regional variations in the AC elastic modulus at 10% nominal strain ($E_{10\%}$). Specifically, C_R of the condyles was significantly higher than C_R of the trochlea, which corresponds with findings of a higher linear elastic modulus on the condyles compared to the trochlea [50,64]. Within the trochlea, C_R of the lateral sub-regions were significantly higher than the central and medial sub-regions. Within the condyles, C_R was higher in the less-weightbearing regions compared to the weightbearing regions. Of note, the linear elastic modulus used as comparison for C_R was computed at 10% nominal strain because the experiment was a strain-driven test and 10% is a typical AC strain during gait. However, we additionally calculated the linear elastic moduli at 1%, 5%, and 15% nominal strain and examined the curvature of the stress–strain plots. From these analyses we confirmed that the trends reported for $E_{10\%}$ would be unaffected if the strain level for calculating the linear modulus was changed.

Please cite this article as: J.M. Deneweth, et al., Hyperelastic modeling of location-dependent human distal femoral cartilage mechanics, International Journal of Non-Linear Mechanics (2014), http://dx.doi.org/10.1016/j.ijnonlinmec.2014.06.013

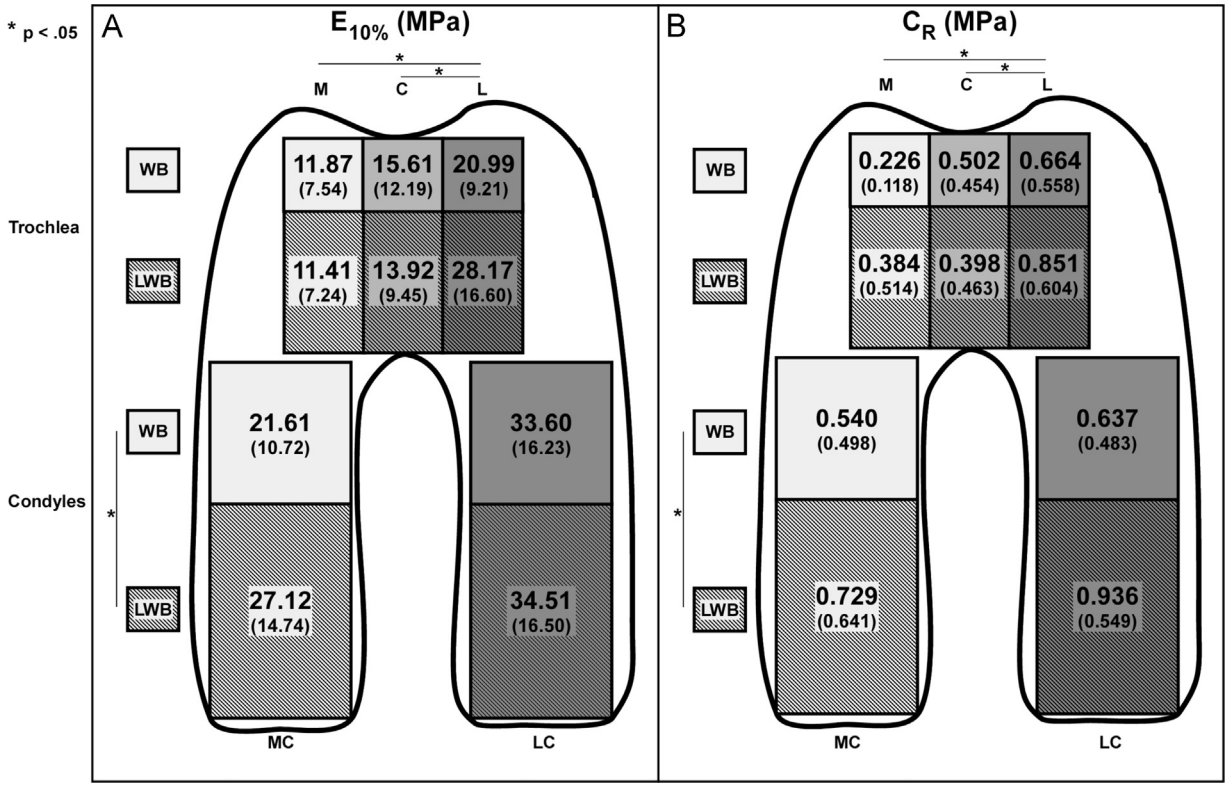

Fig. 8. Comparison of $E_{10\%}$ determined experimentally (A) and C_R from Modified TI model simulations (B). Boxed areas represent each sub-region with text displaying mean (one standard deviation) values of the respective parameter. For both parameters, the medial (M) and central (C) trochlea had significantly lower values ($p < 0.05$) compared to the lateral (L) trochlea. Likewise, mean $E_{10\%}$ and C_R were significantly lower ($p < 0.05$) for the weightbearing (WB) condylar sub-regions compared to the less weightbearing (LWB) condylar sub-regions. LC – lateral condyle, MC – medial condyle. No other statistically significant differences were present between sub-regions.

Little is currently known about regional differences in the collagen structure of femoral AC to relate to the findings of the present study. However, some insight can be drawn from data on the better-researched tibial plateau of the knee. Tibial plateau AC not situated below the menisci exhibits a minimal STZ and is dominated by vertically-oriented collagen fibers [36,65]. This tissue experiences primary loading during walking and running that is generally compressive. In contrast, the AC beneath the menisci has a substantially larger STZ, with collagen fibers predominantly oriented parallel to the cartilage surface [36,65]. It is believed that the meniscus-covered regions are not frequently loaded in gait but rather in tasks requiring deep knee flexion, such as stair climbing and rising from a chair [66]. These tasks involve higher forces than gait [67,68] and also produce more tangentially-oriented (shear) loads on the cartilage due to the sliding and rotating of the femur over the tibia at larger knee flexion angles [69]. It appears, therefore, that regional variations in collagen structure of tibial AC match regional variations in loading patterns. That is, vertically-oriented and less stiff cartilage in regions of lower magnitude but frequently occurring compressive loads and tangentially-oriented, stiffer cartilage in regions of higher magnitude and infrequent shear loads [8,38].

On the femur, similar differences in loading pattern can be defined, which may suggest expectations for the underlying collagen structure. For the femoral condyles, areas of the condyles that contact the tibia joint surfaces between -5° and 30° knee flexion likely experience frequent compressive loading during gait and interact with the low-stiffness, meniscus-uncovered tibial AC [66]. On the other hand, the more posterior/distal portions of the condyles make contact only for knee flexion angles greater than 30°, interact with much stiffer meniscal tissue [70] and meniscus-covered cartilage, and are believed to undergo large, more tangentially-directed loads [59,71]. In this paper these are the WB and LWB regions of the condyles, respectively, and it could be hypothesized that the collagen structure is somewhat similar to the corresponding regions of the tibial plateau. This would agree with the present finding of significantly higher C_R in the LWB compared to the WB regions of the femur condyles.

A similar WB/LWB dichotomy can be inferred from the loading pattern of the trochlea [59,71], but it is complicated by a dominating lateral pull on the patella at low knee flexion angles from the lateral soft tissues of the knee and the quadriceps muscle [72,73]. It also influenced by the flexion-dependent congruency of the patella in the trochlear groove [74]. Inferring collagen structure at the patellofemoral articulation is thus challenging. However, the higher C_R on the lateral third region of the trochlea compared to the central and medial regions may indirectly suggest a collagen structure adapted to concentrated loading of the lateral trochlear aspect. The lack of significant differences between the WB and LWB regions on the trochlea may be due a more complicated trochlea–patella interaction than the relatively simple sliding and rolling of the tibia–femur interaction.

Variations in the mechanical properties of tibiofemoral cartilage [37,50] have been suggested to play an important role in the initiation of OA [75]. However, few cartilage models currently incorporate regionally-varying mechanical properties. The TI model examined herein manifested similar regional mechanical variations to those shown experimentally for healthy human femoral cartilage via only one parameter, C_R. This result indicates that implementing a spatially-dependent C_R in the TI network would allow the spatial heterogeneity of the AC mechanical response to be efficiently represented through a simple collagen-based model within whole joint computational schemes. Fig. 8 provides a starting point for implementing regionally-varying C_R.

While the structure of AC is substantially different from that of the TI model, the mechanistic nature of the model permits some

Please cite this article as: J.M. Deneweth, et al., Hyperelastic modeling of location-dependent human distal femoral cartilage mechanics, International Journal of Non-Linear Mechanics (2014), http://dx.doi.org/10.1016/j.ijnonlinmec.2014.06.013

exploration of potential effects of the collagen matrix on the AC stress–strain response at high strain rates. In the context of knee AC, C_R could be interpreted to partially reflect the volume density of intact collagen fibrils. Areas with fewer collagen fibrils or with increased damage to existing fibrils (e.g., due to OA) are expected to exhibit a lower C_R. The effect of C_R is reflected in the initial modulus of the stress–strain curve; lower C_R dictates a initial modulus [39].

The ratio a:b indicates the extent of transverse isotropy of the collagen matrix: $a:b>1$ occurs when the collagen fibers are more frequently aligned in the direction of compression, and $a:b<1$ occurs when the collagen fibers are preferentially oriented in the plane perpendicular to the compression axis [26]. Collagen fibers in the STZ of knee AC primarily align parallel to the cartilage surface (i.e., perpendicular to the compression axis) [31,36]. The results of this study agree well with this finding as a:b was less than one across all test sites. If a depth-dependent cartilage response is desired, the model could be extended to the entire thickness of the cartilage by allowing a:b to vary with depth: $a:b<1$ in the STZ, $a:b\approx 1$ in the middle zone where the collagen fibers transition from their parallel orientation at the surface to their radial orientation near the subchondral bone, and $a:b>1$ in the deep zone near the subchondral bone [31].

The kinematical variable J governs the compressibility of the tissue. If the tissue is incompressible, meaning that it deforms without changing total volume, $J=1$. Articular cartilage is composed mainly of water and thus is nearly incompressible at high strain rates where negligible fluid flow occurs [47,48]. In the present study J remained nearly constant across regions and knees, which agrees well with the physiology of the tissue and with previous findings for modeling tibial cartilage [32]. Therefore, we feel confident that J can remain fixed near 1 for modeling healthy cartilage. Likewise, changes in the water composition of the tissue or the ability of the tissue to maintain its hydrostatic pressure (e.g., due to severe matrix damage) could be modeled with a decrease in J, although this must first be validated.

We explicitly chose to ignore the proteoglycan content in the model although it influences the compressive loading response of AC [14,19,76,77]. For the short loading duration utilized in our study, negligible fluid flow occurs, negating viscous effects due to the proteoglycan aggregates interacting with fluid flowing out of the tissue [12]. Rather AC deformation occurs under nearly constant volume and is controlled by the resistance of the collagen network [21,78]. We acknowledge that the presence of proteoglycans, by creating an osmotic pressure to resist collapse of the collagen network, enables this deformation to occur [77]. However, it likely does not influence the stress–strain relationship in this case. Bader et al. [22] determined that proteoglycans governed the viscous damping of the compression response while collagen dominated the elastic response. Therefore, in the case of a single unconfined compression loading and immediate unloading, as done in our study, the response should be dominated by the mechanical response of the collagen network. This was confirmed via computational modeling by Li et al. [79]. With these findings in mind we chose to not explicitly consider proteoglycan content. Likewise, the very good fit of the model is possible because of the minimal influence of proteoglycan in the loading scenario utilized. Additionally, this finding is likely possible because we strictly examined healthy tissue. Osteoarthritic tissue is known to have higher proteoglycan content, increased swelling, and a compromised collagen structure [76,80]. In this case, it is possible that negligible fluid flow may not be a valid assumption and proteoglycan content must be considered.

The mean R^2 for the TI model with all parameters fixed except C_R was very high, but 20% of the simulations were subsequently rejected for $R^2<0.97$. Post-hoc repeated-measures ANOVA determined that mean b for high-rejection test sites (50% or more rejected trials) was 1.287, which was significantly lower than mean b for low-rejection sites ($b=1.325$), $F(1,6)=325.95$, $p<0.001$. This finding suggests that the model is particularly sensitive to b in regions with less anisotropy than average (i.e., lower b). Nonetheless all rejected simulations demonstrated $R^2>0.90$, which is generally accepted as a high goodness of fit. When the regional analysis for C_R was repeated with all simulations included, observed regional variations in C_R remained the same. Consequently, the modified TI model would be an excellent method for modeling the high strain-rate response of femoral AC.

Several potential limitations may impact the generalizability of study outcomes. The experimental data used for this study, for example, were taken from a restricted demographic. It is therefore unclear as to the extent to which these results can be applied to the general population. Further work must be done to validate the model against datasets from other demographics and if necessary determine relevant parameter values for these groups. The model has also only been evaluated for AC loaded in unconfined compression, but other deformation states, e.g., shear, may also be relevant to cartilage degeneration. Eight-chain networks have successfully modeled multiple deformation states for polymers [34,39], but this has not been examined with AC. Additional research into the extent to which the current model parameters can successfully simulate other important deformation states should now be conducted. Nonetheless, the TI model appears to be highly valuable for modeling of AC within whole-knee computational models. Several elegant non-linear, inhomogeneous, anisotropic cartilage models currently exist, but few model topographical variations in cartilage mechanics and none with a single varying-parameter as in the TI model [57,81-88]. Modeling cartilage with the TI model will provide new insights into diseases associated with the non-uniform mechanical properties of the tissue without compromising the efficient dynamics of the whole model. If such steps are taken, efforts to implement and validate the TI model using a region-dependent C_R, within a valid knee joint model, should initially be undertaken.

The TI model as proposed in this paper can feasibly be implemented within any commercial finite element package that permits user-defined hyperelastic materials (e.g., Abaqus, Dassault Systèmes, France). The model's strain energy Eq. (11) would be supplied along with its derivatives and parameter values. The strain energy can be simplified by using constant values for all parameters except C_R (i.e., $nk\theta$): $\alpha,a,J,B=1$; and $b=1.3481$. To model the heterogeneity in human AC, C_R must be defined as a function of position across the cartilage surface (Fig. 8). The TI model is appropriate for any material with known transverse anisotropy and a mechanical response primarily dictated by non-linear, recoverable deformation.

5. Conclusions

Three statistical chain network models have been evaluated for simulating high strain-rate uniaxial compression of healthy human femoral AC. The TI model was found to most successfully fit the data. Moreover, the model maintained an excellent fit when its degrees of freedom were reduced from three to one, which is not common for a mechanistic cartilage model. The reduced degree of freedom TI model was particularly novel in that regional variations in its single non-constant parameter, C_R, followed the same pattern as experimentally-measured elastic modulus. The model incorporates parameters that could be interpreted with respect to the collagen structure of the AC. This mechanistic nature along with its efficient formulation make it particularly valuable for implementing into computational models of the knee. Furthermore, its ability to simulate the regionally-varying properties of

Please cite this article as: J.M. Deneweth, et al., Hyperelastic modeling of location-dependent human distal femoral cartilage mechanics, International Journal of Non-Linear Mechanics (2014), http://dx.doi.org/10.1016/j.ijnonlinmec.2014.06.013

healthy knee cartilage, which is currently not replicated by other models, will greatly enhance current investigations of knee OA initiation and progression.

Acknowledgments

The authors gratefully acknowledge Ms. K. Newman, Ms. S. Pomeroy, and Mr. S. Sylvia for their assistance with data acquisition. J.M.D. was supported by the Department of Defense through the National Defense Science & Engineering Graduate Fellowship Program while conducting this research. E.M.A. would like to thank Ray Ogden, Giuseppe Saccomandi, and Alan Wineman for inviting her to contribute to this special issue in honor of Alan Gent.

References

[1] R.C. Lawrence, D.T. Felson, C.G. Helmick, L.M. Arnold, H. Choi, R.A. Deyo, S. Gabriel, R. Hirsch, M.C. Hochberg, G.G. Hunder, J.M. Jordan, J.N. Katz, H. M. Kremers, F. Wolfe, Estimates of the prevalence of arthritis and other rheumatic conditions in the United States. Part II, Arthritis Rheum. 58 (1) (2008) 26–35.
[2] R. Shirazi, A. Shirazi-Adl, Analysis of partial meniscectomy and ACL reconstruction in knee joint biomechanics under a combined loading, Clin. Biomech. 24 (9) (2009) 755–761.
[3] J.Y. Bae, K.S. Park, J.K. Seon, D.S. Kwak, I. Jeon, E.K. Song, Biomechanical analysis of the effects of medial meniscectomy on degenerative osteoarthritis, Med. Biol. Eng. Comput. 50 (1) (2012) 53–60.
[4] E. Pena, B. Calvo, M.A. Martinez, D. Palanca, M. Doblare, Why lateral meniscectomy is more dangerous than medial meniscectomy. A finite element study, J. Orthop. Res. 24 (5) (2006) 1001–1010.
[5] W. Wilson, C.C. van Donkelaar, R. van Rietbergen, R. Huiskes, The role of computational models in the search for the mechanical behavior and damage mechanisms of articular cartilage, Med. Eng. Phys. 27 (10) (2005) 810–826.
[6] Z.A. Taylor, K. Miller, Constitutive modeling of cartilaginous tissues: a review, J. Appl. Biomech. 22 (3) (2006) 212–229.
[7] M. Hubbard, Computer simulation in sport and industry, J. Biomech. 26 (Suppl. 1) (1993) 53–61.
[8] T.P. Andriacchi, S. Koo, S.F. Scanlan, Gait mechanics influence healthy cartilage morphology and osteoarthritis of the knee, J. Bone Jt. Surg. Am. 91 (2 Suppl. 1) (2009) 95–101.
[9] T.P. Andriacchi, A. Mundermann, The role of ambulatory mechanics in the initiation and progression of knee osteoarthritis, Curr. Opin. Rheumatol. 18 (5) (2006) 514–518.
[10] F. Liu, M. Kozanek, A. Hosseini, S.K. Van de Velde, T.J. Gill, H.E. Rubash, G. Li, In vivo tibiofemoral cartilage deformation during the stance phase of gait, J. Biomech. 43 (4) (2010) 658–665.
[11] R.A. Mann, J. Hagy, Biomechanics of walking, running, and sprinting, Am. J. Sports Med. 8 (5) (1980) 345–350.
[12] C.G. Armstrong, W.M. Lai, V.C. Mow, An analysis of the unconfined compression of articular cartilage, J. Biomech. Eng. 106 (2) (1984) 165–173.
[13] M.R. DiSilvestro, Q. Zhu, J.K. Suh, Biphasic poroviscoelastic simulation of the unconfined compression of articular cartilage: II—Effect of variable strain rates, J. Biomech. Eng. 123 (2) (2001) 198–200.
[14] V.C. Mow, X.E. Guo, Mechano-electrochemical properties of articular cartilage: their inhomogeneities and anisotropies, Annu. Rev. Biomed. Eng. 4 (2002) 175–209.
[15] X.L. Lu, V.C. Mow, Biomechanics of articular cartilage and determination of material properties, Med. Sci. Sports Exerc. 40 (2) (2008) 193–199.
[16] E.H. Han, S.S. Chen, S.M. Klisch, R.L. Sah, Contribution of proteoglycan osmotic swelling pressure to the compressive properties of articular cartilage, Biophys. J. 101 (4) (2011) 916–924.
[17] X.L. Lu, V.C. Mow, X.E. Guo, Proteoglycans and mechanical behavior of condylar cartilage, J. Dent. Res. 88 (3) (2009) 244–248.
[18] D.D. Sun, X.E. Guo, M. Likhitpanichkul, W.M. Lai, V.C. Mow, The influence of the fixed negative charges on mechanical and electrical behaviors of articular cartilage under unconfined compression, J. Biomech. Eng. 126 (1) (2004) 6–16.
[19] V.C. Mow, M.H. Holmes, W.M. Lai, Fluid transport and mechanical properties of articular cartilage: a review, J. Biomech. 17 (5) (1984) 377–394.
[20] D.L. Bader, G.E. Kempson, J. Egan, W. Gilbey, A.J. Barrett, The effects of selective matrix degradation on the short-term compressive properties of adult human articular cartilage, Biochim. Biophys. Acta 1116 (2) (1992) 147–154.
[21] J. Mizrahi, A. Maroudas, Y. Lanir, I. Ziv, T.J. Webber, The instantaneous deformation of cartilage: effects of collagen fiber orientation and osmotic stress, Biorheology 23 (4) (1986) 311–330.
[22] D.L. Bader, G.E. Kempson, The short-term compressive properties of adult human articular cartilage, Biomed. Mater. Eng. 4 (3) (1994) 245–256.
[23] A.I. Maroudas, Balance between swelling pressure and collagen tension in normal and degenerate cartilage, Nature 260 (5554) (1976) 808–809.
[24] E. Gentleman, A.N. Lay, D.A. Dickerson, E.A. Nauman, G.A. Livesay, K.C. Dee, Mechanical characterization of collagen fibers and scaffolds for tissue engineering, Biomaterials 24 (21) (2003) 3805–3813.
[25] L.P. Li, K.B. Gu, Reconsideration on the use of elastic models to predict the instantaneous load response of the knee joint, Proc. Inst. Mech. Eng. H 225 (9) (2011) 888–896.
[26] J.E. Bischoff, E.M. Arruda, K. Grosh, A microstructurally based orthotropic hyperelastic constitutive law, J. Appl. Mech.-Trans. ASME 69 (5) (2002) 570–579.
[27] J.E. Bischoff, E.M. Arruda, K. Grosh, A rheological network model for the continuum anisotropic and viscoelastic behavior of soft tissue, Biomech. Model. Mechanobiol. 3 (1) (2004) 56–65.
[28] E. Kühl, K. Garikipati, E.M. Arruda, K. Grosh, Remodeling of biological tissue: mechanically induced reorientation of a transversely isotropic chain network, J. Mech. Phys. Solids 53 (7) (2005) 1552–1573.
[29] J. Ma, H. Narayanan, K. Garikipati, K. Grosh, E.M. Arruda, Experimental and computational investigation of viscoelasticity of native and engineered ligament and tendon, in: Iutam Symposium on Cellular, Molecular and Tissue Mechanics, Proceedings, Springer, New York (2010) 3–17.
[30] E.M. Hasler, W. Herzog, J.Z. Wu, W. Muller, U. Wyss, Articular cartilage biomechanics: theoretical models, material properties, and biosynthetic response, Crit. Rev. Biomed. Eng. 27 (6) (1999) 415–488.
[31] A.K. Jeffery, G.W. Blunn, C.W. Archer, G. Bentley, Three-dimensional collagen architecture in bovine articular cartilage, J. Bone Jt. Surg. Br. 73 (5) (1991) 795–801.
[32] J.M. Deneweth, S.G. McLean, E.M. Arruda, Evaluation of hyperelastic models for the non-linear and non-uniform high strain-rate mechanics of tibial cartilage, J. Biomech. (2013) (published online May 12, 2013).
[33] J.S. Palmer, M.C. Boyce, Constitutive modeling of the stress–strain behavior of F-actin filament networks, Acta Biomater. 4 (3) (2008) 597–612.
[34] M.C. Boyce, E.M. Arruda, Constitutive models of rubber elasticity: a review, Rubber Chem. Technol. 73 (3) (2000) 504–523.
[35] A.N. Gent, New constitutive relation for rubber, Rubber Chem. Technol. 69 (1) (1996) 59.
[36] J.M. Clark, Variation of collagen fiber alignment in a joint surface: a scanning electron microscope study of the tibial plateau in dog, rabbit, and man, J. Orthop. Res. 9 (2) (1991) 246–257.
[37] J.M. Deneweth, K.E. Newman, S.M. Sylvia, S.G. McLean, E.M. Arruda, Heterogeneity of tibial plateau cartilage in response to a physiological compressive strain rate, J. Orthop. Res. 31 (3) (2013) 370–375.
[38] A.M. Chaudhari, P.L. Briant, S.L. Bevill, S. Koo, T.P. Andriacchi, Knee kinematics, cartilage morphology, and osteoarthritis after ACL injury, Med. Sci. Sports Exerc. 40 (2) (2008) 215–222.
[39] E.M. Arruda, M.C. Boyce, A 3-dimensional constitutive model for the large stretch behavior of rubber elastic—materials, J. Mech. Phys. Solids 41 (2) (1993) 389–412.
[40] F.C. MacKintosh, J. Kas, P.A. Janmey, Elasticity of semiflexible biopolymer networks, Phys. Rev. Lett. 75 (24) (1995) 4425–4428.
[41] W. Kühn, F. Grun, Relations between elastic constants and the strain birefringence of high-elastic substances, Kolloid-Z. 101 (3) (1942) 248–271.
[42] A. Cohen, A Pade approximant to the inverse Langevin function, Rheol. Acta 30 (3) (1991) 270–273.
[43] J.E. Bischoff, E.M. Arruda, K. Grosh, Finite element modeling of human skin using an isotropic, nonlinear elastic constitutive model, J. Biomech. 33 (6) (2000) 645–652.
[44] Y. Liu, A. Kerdok, R. Howe, A nonlinear finite element model of soft tissue indentation, Med. Simul. (2004) 67–76.
[45] C.P. Brown, T.C. Nguyen, H.R. Moody, R.W. Crawford, A. Oloyede, Assessment of common hyperelastic constitutive equations for describing normal and osteoarthritic articular cartilage, Proc. Inst. Mech. Eng. H 223 (H6) (2009) 643–652.
[46] V.C. Mow, S.C. Kuei, W.M. Lai, C.G. Armstrong, Biphasic creep and stress relaxation of articular cartilage in compression? Theory and experiments, J. Biomech. Eng. 102 (1) (1980) 73–84.
[47] G.A. Ateshian, B.J. Ellis, J.A. Weiss, Equivalence between short-time biphasic and incompressible elastic material responses, J. Biomech. Eng. 129 (3) (2007) 405–412.
[48] M. Wong, M. Ponticiello, V. Kovanen, J.S. Jurvelin, Volumetric changes of articular cartilage during stress relaxation in unconfined compression, J. Biomech. 33 (9) (2000) 1049–1054.
[49] J.E. Bischoff, E.M. Arruda, K. Grosh, Orthotropic hyperelasticity in terms of an arbitrary molecular chain model, J. Appl. Mech.-Trans. ASME, 69, 2002 198–201.
[50] A.C. Swann, B.B. Seedhom, The stiffness of normal articular cartilage and the predominant acting stress levels: implications for the aetiology of osteoarthrosis, Br. J. Rheumatol. 32 (1) (1993) 16–25.
[51] R.J. Lewis, A.K. MacFarland, S. Anandavijayan, R.M. Aspden, Material properties and biosynthetic activity of articular cartilage from the bovine carpometacarpal joint, Osteoarthr. Cartil. 6 (6) (1998) 383–392.
[52] R. Krishnan, S. Park, F. Eckstein, G.A. Ateshian, Inhomogeneous cartilage properties enhance superficial interstitial fluid support and frictional properties, but do not provide a homogeneous state of stress, J. Biomech. Eng. 125 (5) (2003) 569–577.
[53] S. Ronken, M.P. Arnold, H. Ardura Garcia, A. Jeger, A.U. Daniels, D. Wirz, A comparison of healthy human and swine articular cartilage dynamic indentation mechanics, Biomech. Model. Mechanobiol. 11 (5) (2012) 631–639.
[54] G. Meachim, Light microscopy of Indian ink preparations of fibrillated cartilage, Ann. Rheum. Dis. 31 (6) (1972) 457–464.

Please cite this article as: J.M. Deneweth, et al., Hyperelastic modeling of location-dependent human distal femoral cartilage mechanics, International Journal of Non-Linear Mechanics (2014), http://dx.doi.org/10.1016/j.ijnonlinmec.2014.06.013

[55] J. Ma, M.J. Smietana, T.Y. Kostrominova, E.M. Wojtys, L.M. Larkin, E.M. Arruda, Three-dimensional engineered bone–ligament–bone constructs for anterior cruciate ligament replacement, Tissue Eng. Part A 18 (1–2) (2012) 103–116.
[56] J. Ma, K. Goble, M. Smietana, T. Kostrominova, L. Larkin, E.M. Arruda, Morphological and functional characteristics of three-dimensional engineered bone–ligament–bone constructs following implantation, J. Biomech. Eng. 131 (10) (2009) 101017.
[57] S. Chegini, S.J. Ferguson, Time and depth dependent Poisson's ratio of cartilage explained by an inhomogeneous orthotropic fiber embedded biphasic model, J. Biomech. 43 (9) (2010) 1660–1666.
[58] R.K. Korhonen, M.S. Laasanen, J. Toyras, J. Rieppo, J. Hirvonen, H.J. Helminen, J. S. Jurvelin, Comparison of the equilibrium response of articular cartilage in unconfined compression, confined compression and indentation, J. Biomech. 35 (7) (2002) 903–909.
[59] J. Goodfellow, D.S. Hungerford, M. Zindel, Patello-femoral joint mechanics and pathology. 1. Functional anatomy of the patello-femoral joint, J. Bone Jt. Surg. Br. 58 (3) (1976) 287–290.
[60] A. Garg, P.S. Walker, Prediction of total knee motion using a three-dimensional computer-graphics model, J. Biomech. 23 (1) (1990) 45–58.
[61] J.A. Feller, A.A. Amis, J.T. Andrish, E.A. Arendt, P.J. Erasmus, C.M. Powers, Surgical biomechanics of the patellofemoral joint, Arthroscopy 23 (5) (2007) 542–553.
[62] G. Li, S.E. Park, L.E. DeFrate, M.E. Schutzer, L. Ji, T.J. Gill, H.E. Rubash, The cartilage thickness distribution in the tibiofemoral joint and its correlation with cartilage-to-cartilage contact, Clin. Biomech. 20 (7) (2005) 736–744.
[63] D. Eyre, Collagen of articular cartilage, Arthritis Res. 4 (1) (2002) 30–35.
[64] M.K. Barker, B.B. Seedhom, The relationship of the compressive modulus of articular cartilage with its deformation response to cyclic loading: does cartilage optimize its modulus so as to minimize the strains arising in it due to the prevalent loading regime? Rheumatology 40 (3) (2001) 274–284.
[65] D.R. Eyre, M.A. Weis, J.J. Wu, Articular cartilage collagen: an irreplaceable framework? Eur. Cells Mater. 12 (2006) 57–63.
[66] J.T. Bingham, R. Papannagari, S.K. Van de Velde, C. Gross, T.J. Gill, D.T. Felson, H. E. Rubash, G. Li, In vivo cartilage contact deformation in the healthy human tibiofemoral joint, Rheumatology 47 (11) (2008) 1622–1627.
[67] I.G. Goudakos, C. Konig, P.B. Schottle, W.R. Taylor, N.B. Singh, I. Roberts, F. Streitparth, G.N. Duda, M.O. Heller, Stair climbing results in more challenging patellofemoral contact mechanics and kinematics than walking at early knee flexion under physiological-like quadriceps loading, J. Biomech. 42 (15) (2009) 2590–2596.
[68] B.B. Seedhom, K. Terayama, Knee forces during the activity of getting out of a chair with and without the aid of arms, Biomed. Eng. 11 (8) (1976) 278–282.
[69] M.A. Lafortune, P.R. Cavanagh, H.J. Sommer III, A. Kalenak, Three-dimensional kinematics of the human knee during walking, J. Biomech. 25 (4) (1992) 347–357.
[70] H.N. Chia, M.L. Hull, Compressive moduli of the human medial meniscus in the axial and radial directions at equilibrium and at a physiological strain rate, J. Orthop. Res. 26 (7) (2008) 951–956.
[71] T.M. van Eijden, E. Kouwenhoven, J. Verburg, W.A. Weijs, A mathematical model of the patellofemoral joint, J. Biomech. 19 (3) (1986) 219–229.
[72] C.M. Powers, F.G. Shellock, M. Pfaff, Quantification of patellar tracking using kinematic MRI, J. Magn. Reson. Imaging 8 (3) (1998) 724–732.
[73] S.K. Han, S. Federico, M. Epstein, W. Herzog, An articular cartilage contact model based on real surface geometry, J. Biomech. 38 (1) (2005) 179–184.
[74] V.V. Patel, K. Hall, M. Ries, C. Lindsey, E. Ozhinsky, Y. Lu, S. Majumdar, Magnetic resonance imaging of patellofemoral kinematics with weight-bearing, 19182033, 85-A(12), 2003, pp. 2419–2424.
[75] T.P. Andriacchi, A. Mundermann, R.L. Smith, E.J. Alexander, C.O. Dyrby, S. Koo, A framework for the in vivo pathomechanics of osteoarthritis at the knee, Ann. Biomed. Eng. 32 (3) (2004) 447–457.
[76] C.G. Armstrong, V.C. Mow, Variations in the intrinsic mechanical properties of human articular cartilage with age, degeneration, and water content, J. Bone Jt. Surg. Am. 64 (1) (1982) 88–94.
[77] I.M. Basalo, R.L. Mauck, T.A. Kelly, S.B. Nicoll, F.H. Chen, C.T. Hung, G. A. Ateshian, Cartilage interstitial fluid load support in unconfined compression following enzymatic digestion, J. Biomech. Eng. 126 (6) (2004) 779–786.
[78] C.J. Moger, K.P. Arkill, R. Barrett, P. Bleuet, R.E. Ellis, E.M. Green, C.P. Winlove, Cartilage collagen matrix reorientation and displacement in response to surface loading, J. Biomech. Eng. 131 (3) (2009) 031008.
[79] L.P. Li, M.D. Buschmann, A. Shirazi-Adl, Strain-rate dependent stiffness of articular cartilage in unconfined compression, J. Biomech. Eng. 125 (2) (2003) 161–168.
[80] L. Hendren, P. Beeson, A review of the differences between normal and osteoarthritis articular cartilage in human knee and ankle joints, Foot 19 (3) (2009) 171–176.
[81] W. Wilson, J.M. Huyghe, C.C. van Donkelaar, A composition-based cartilage model for the assessment of compositional changes during cartilage damage and adaptation, Osteoarthr. Cartil. 14 (6) (2006) 554–560.
[82] W. Wilson, C.C. van Donkelaar, B. van Rietbergen, K. Ito, R. Huiskes, Stresses in the local collagen network of articular cartilage: a poroviscoelastic fibril-reinforced finite element study, J. Biomech. 37 (3) (2004) 357–366.
[83] L.P. Li, J. Soulhat, M.D. Buschmann, A. Shirazi-Adl, Nonlinear analysis of cartilage in unconfined ramp compression using a fibril reinforced poroelastic model, Clin. Biomech. 14 (9) (1999) 673–682.
[84] M.J. Askew, V.C. Mow, Biomechanical function of the collagen fibril ultra-structure of articular cartilage, J. Biomech. Eng. 100 (3) (1978) 105–115.
[85] G.A. Ateshian, V. Rajan, N.O. Chahine, C.E. Canal, C.T. Hung, Modeling the matrix of articular cartilage using a continuous fiber angular distribution predicts many observed phenomena, J. Biomech. Eng. 131 (6) (2009) 061003.
[86] N.M. Bachrach, V.C. Mow, F. Guilak, Incompressibility of the solid matrix of articular cartilage under high hydrostatic pressures, J. Biomech. 31 (5) (1998) 445–451.
[87] L.P. Li, W. Herzog, R.K. Korhonen, J.S. Jurvelin, The role of viscoelasticity of collagen fibers in articular cartilage: axial tension versus compression, Med. Eng. Phys. 27 (1) (2005) 51–57.
[88] M.A. Soltz, G.A. Ateshian, A Conewise Linear Elasticity mixture model for the analysis of tension-compression nonlinearity in articular cartilage, J. Biomech. Eng. 122 (6) (2000) 576–586.

Please cite this article as: J.M. Deneweth, et al., Hyperelastic modeling of location-dependent human distal femoral cartilage mechanics, International Journal of Non-Linear Mechanics (2014), http://dx.doi.org/10.1016/j.ijnonlinmec.2014.06.013